

1 Density Functional Theory Study on the Coupling and Reactions of Diferuloylputrescine as a
2 Lignin Monomer

3

4 Thomas Elder,*¹ José C. del Río,² John Ralph,^{3,4} Jorge Rencoret,² and Hoon Kim³

5

6 ¹USDA-Forest Service, Southern Research Station, 521 Devall Drive, Auburn, AL 36849, USA

7 ²Instituto de Recursos Naturales y Agrobiología de Sevilla (IRNAS), CSIC, Av. Reina Mercedes,
8 10, 41012-Seville, Spain

9 ³Department of Energy Great Lakes Bioenergy Research Center, Wisconsin Energy Institute,
10 University of Wisconsin, 1552 University Ave, Madison, WI 53726, USA

11 ⁴Department of Biochemistry, University of Wisconsin, 433 Babcock Drive, Madison, WI
12 53706, USA

13

14 * Corresponding Author

15 E-mail address: thomas.elder@usda.gov

16 (t) 334-826-7800 x 148

17 (f) 334-821-0037

18

19

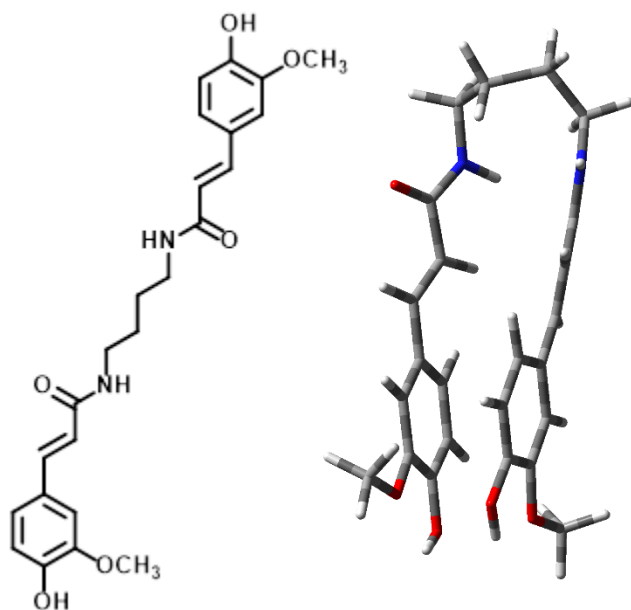
20

21 **Abstract**

22
23 Diferuloylputrescine has been found in a variety of plant species, and recent work has provided
24 evidence of its covalent bonding into lignin. Results from nuclear magnetic resonance
25 spectroscopy revealed the presence of bonding patterns consistent with homo-coupling of
26 diferuloylputrescine and the possibility of cross-coupling with lignin. In the present work,
27 density functional theory calculations have been applied to assess the energetics associated with
28 radical coupling, rearomatization, and dehydrogenation for possible homo-coupled dimers of
29 diferuloylputrescine and cross-coupled dimers of diferuloylputrescine and coniferyl alcohol. The
30 values obtained for these reaction energetics are consistent with those reported for monolignols
31 and other novel lignin monomers. As such, this study shows that there would be no
32 thermodynamic impediment to the incorporation of diferuloylputrescine into the lignin polymer
33 and its addition to the growing list of non-canonical lignin monomers.

34 **Graphical abstract**

35



Diferuloylputrescine

36

37 Low energy conformation for isolated diferuloylputrescine.

38 **Keywords**

39

40 Diferuloylputrescine, homo-couple, cross-couple, density functional theory, coniferyl alcohol,
41 lignin, lignification, feruloyl amide, radical coupling

42

43 **Highlights**

44

45 • Density functional theory calculations have been performed on diferuloylputrescine
46 and its reaction products

47

48 • The thermodynamic feasibility of coupling reactions of diferuloylputrescine are
49 demonstrated

50

51 • The dehydrogenation of diferuloylputrescine dimers is energetically compatible with
52 lignols, demonstrating the feasibility of incorporation into the lignin polymer

53

54

55 **1. Introduction**

56 The plasticity of lignification towards the incorporation of monomers from beyond the canonical
57 hydroxycinnamyl alcohols (the monolignols coniferyl, sinapyl, and *p*-coumaryl alcohol) has been
58 repeatedly demonstrated and recently reviewed (del Río et al., 2021, 2020; Ralph et al., 2021).

59 At last report there were 35 monomers that may occur naturally or are produced due to genetic
60 modifications (either natural or induced) that have been found in natural lignins (Ralph et al.,
61 2019; Vanholme et al., 2019). Included are monolignol ester conjugates (with ferulates, acetates,
62 *p*-hydroxybenzoates, *p*-coumarates, vanillates, or benzoates) (del Río et al., 2008, 2007; Karlen
63 et al., 2017, 2016; Kim et al., 2020; Lu et al., 2015), the catechyl alcohols (caffeyl and 5-
64 hydroxyconiferyl alcohol) (Chen et al., 2012; Ralph et al., 2001), and dihydroconiferyl alcohol
65 and hydroxycinnamaldehydes (Ralph et al., 1997), all of which are derived from the general
66 phenylpropanoid pathway. Subsequently, lignin monomers arising from other metabolic
67 pathways (i.e., a hybrid of the phenylpropanoid and acetate/malonate polyketide pathway or the
68 amino acid pathway) have been identified (del Río et al., 2021, 2020). These include the

69 hydroxystilbenes and their glucosylated derivatives (del Río et al., 2017; Rencoret et al., 2019,
70 2018), the flavone tricetin (del Río et al., 2012; Lan et al., 2016b, 2016a, 2015), the nitrogen-
71 containing feruloyltyramine, and the subject of the current paper diferuloylputrescine (del Río et
72 al., 2018; Kudanga et al., 2009; Negrel et al., 1996; Ralph et al., 1998).

73
74 Diferuloylputrescine (Figure 1) has been found in extracts from corn (*Zea mays*) and corn oil
75 (Moreau et al., 2001; Moreau and Hicks, 2005), as well as in bamboo (*Phyllostachys*
76 *heterocycla*) (Yoshimura et al., 2017). Beyond botanical interest, diferuloylputrescine has been
77 found to be quite active biologically. In a study of antiprotozoal activity, diferuloylputrescine
78 was found in the chloroform extracts of *Haplophyllum tuberculatum* roots; among the
79 compounds isolated it was found to be the most effective against *Trypanosoma brucei*
80 *rhodesiense*, which causes sleeping sickness (Mahmoud et al., 2020). Other work on extracts
81 from corn has found that diferuloylputrescine has high antioxidant activity (Bauer et al., 2013,
82 2012), anti-inflammatory and anti-melanogenic properties (Kim et al., 2012, 2010), inhibits
83 aflatoxin production (Mellon and Moreau, 2004), and is inhibitory to α -glucosidase, a property
84 that can have applications in diabetes treatments (Niwa et al., 2003).

85
86 In a study on the milled wood lignin (MWL) and dioxane lignin (DL) preparations isolated from
87 corn grain fibers, the presence of diferuloylputrescine was detected by the application of 2D
88 HSQC NMR (del Río et al., 2018). The detailed assignments demonstrating the occurrence of
89 diferuloylputrescine were determined by 2D HSQC-TOCSY and HMBC NMR experiments. The
90 latter are consistent with literature spectra and have been confirmed with a synthetically prepared
91 authentic standard. As discussed previously, free diferuloylputrescine can be extracted with

92 organic solvents, and the corn fiber in the referenced paper had been subjected to exhaustive
93 extraction with acetone, methanol and water. This demonstrated that the diferuloylputrescine
94 detected in the isolated lignins was covalently bonded to the cell wall and was not a residual free
95 compound. The NMR experiments also provided evidence of 8-5' phenylcoumaran linkages
96 involving diferuloylputrescine, showing that homo-coupled dimers or higher oligomers may
97 occur along with the possibility of cross-coupling to ferulates or lignin. Feruloyl amides, which
98 include diferuloylputrescine, are substrates for peroxidase enzymes *in vitro* such that the
99 resultant phenoxy radicals (Figure 1) could couple through the 5-, 8- and 4-O- positions by
100 radical addition to another diferuloylputrescine, ferulates, or monolignols, followed by
101 rearomatization, becoming integrated into the cell wall. Based on these possible reactive sites,
102 diferuloylputrescine could act as a branch point within the lignin polymer, resulting in a cross-
103 linked network and, as two phenolic groups are present, lignification could occur at both
104 phenolic ends.

105
106 To date, the 8-5' linkage has been unambiguously identified, whereas other potential coupling
107 products, such as 8-O-4' or 5-5', have only been tentatively identified by NMR and await
108 confirmation. The objective of the current work is therefore to determine if the reactions required
109 for the formation of the homo-coupled and cross-coupled products are energetically feasible.
110 This question will be addressed by the application of contemporary methods in computational
111 chemistry to the proposed reactants and products associated with homo-coupling of
112 diferuloylputrescine and its cross-coupling with monolignols. In addition, given the documented
113 medicinal value of diferuloylputrescine, its release from plant tissues may provide a new source
114 of this compound. As such, the bond dissociation energies of the homo-coupled and cross-

115 coupled dimers will be determined to assess the potential for liberation of diferuloylputrescine.
116 Furthermore, as the dimers have at least two phenolic groups, and could potentially react through
117 all of them, the energy associated with dehydrogenation at these points will be determined. The
118 computational work flow described in the current submission involving a force-field-based
119 conformational search followed by refinement with one or more electronic structure methods is
120 consistent with previously published papers (by ourselves and others) concerned with the
121 conformation and reactivity of isolated lignin structures. This process has undergone extensive
122 peer review and has also been successfully applied to the non-canonical lignin monomers
123 piceatannol, triclin, and the catechyl alcohols. (Berstis et al., 2020, 2016; Elder et al., 2020, 2019,
124 2016; Kim et al., 2011; Sangha et al., 2014, 2012).

125

126

127 **2. Results and Discussion**

128 **2.1 *Dehydrogenation of diferuloylputrescine***

129 The energy of diferuloylputrescine dehydrogenation (Figure 1) at 76.6 kcal mol⁻¹ is comparable
130 to that of the canonical monolignols (coniferyl alcohol, 77.1 kcal mol⁻¹; sinapyl alcohol, 72.8
131 kcal mol⁻¹; *p*-coumaryl alcohol, 76.4 kcal mol⁻¹), as well as other non-conventional lignin
132 monomers such as piceatannol (76.4 kcal mol⁻¹) (Elder et al., 2019) and the hydroxystilbene
133 glucosides (75.8–76.8 kcal mol⁻¹) (Elder et al., 2021). The optimized structures of
134 diferuloylputrescine and its dehydrogenation product are shown in Figure 2. The most striking
135 observation of the monomer and radical structures is the markedly folded conformations in
136 which the aromatic rings are at distances of 3.60 and 3.58 Å, respectively. The rings are also
137 essentially parallel with an inter-plane angle of 6.72° for the diferuloylputrescine and 4.87° for

138 the radical. These conformations and inter-ring distances are consistent with the sandwich
139 geometry of aromatic dimers in which π -stacking is proposed to occur (Sinnokrot and Sherrill,
140 2004). Figure 2 also shows that the locations of unpaired spin density of the diferuloylputrescine
141 radical are consistent with the predicted resonance structures in Figure 1 and with those of the
142 monolignols.

143
144 It should also be noted that these observed geometries are the result of gas phase calculations.
145 The conformations were further investigated with implicit solvation with water, resulting in the
146 structures shown in Figure 2. It can be seen that the folded geometry is retained upon solvation
147 for both the closed-shell and radical forms of diferuloylputrescine.

148

149 ***2.2 Radical coupling and rearomatization***

150 *2.2.1 Homo-coupled diferuloylputrescine*

151 The free energies of radical coupling and rearomatization for the several homo-coupled dimers
152 are as shown in Figure 3. Among the intermediates resulting from the radical coupling step, the
153 8-O-4' quinone methide is the most stable and therefore its formation is the most exergonic. The
154 radical coupling step in this case generates a single new chiral center. Among the 8-5' quinone
155 methide and the 5-5' di-cyclohexadienone intermediates, both of which involve carbon-carbon
156 bond formation, the latter intermediates that involve two aromatic centers, are less stable by ~6–
157 12 kcal mol⁻¹. These lowered stabilities can be attributed to larger reductions in aromaticity upon
158 coupling. Radical coupling through the 8-5' and 5-5' positions generates two chiral centers each,
159 for which there is some degree of stereochemical preference at 4.2 and 2.2 kcal mol⁻¹,
160 respectively.

161
162 The rearomatization reactions follow a predictable pattern with the 5-5' dimer, which involves
163 carbon-carbon bond formation, as the most exergonic, and the carbon-oxygen bonded 8-O-4', as
164 the least. The 8-5' product in which both carbon-carbon and carbon-oxygen bonds are formed
165 along with ring closure varies with stereochemistry, wherein the *RS/SR* stereoisomer, is the most
166 stable of the dimeric products, although the difference with 5-5' (0.6 kcal mol⁻¹) is within the
167 accuracy of the density functional theory method used in this work (0.4-1.3 kcal mol⁻¹) (Zhao
168 and Truhlar, 2008), such that they cannot be differentiated based on energy. Furthermore, the
169 low energy *RS/SR* stereoisomer of the 8-5' dimer corresponds to the *cis* conformation, rather than
170 the *trans* configuration routinely found in lignin structures (Li et al., 1997; Ralph et al., 2009).

171
172 The optimized geometries of the dimers (Figure 2) are predictably more complex than the
173 monomer, but also exhibit folded conformations. The 8-O-4' and 8-5'-*SS/RR* are twisted and
174 irregular, whereas the aromatic rings of the 5-5' and 8-5'-*SR/RS* dimers are in close proximity
175 and fairly parallel. Within the 5-5' dimer, the torsional angle between rings A and B is 35.21°,
176 the inter-ring distances for rings B-D and A-C are 3.50 and 3.87 Å, with plane angles of 6.62
177 15.97°, respectively. The C-D ring combination of the 8-5'-*SR* is separated by 3.50 Å, with a
178 plane angle of 13.48°. Based on these observations and the differences in energies, stacking of
179 the aromatic rings appears to be contributing to the higher stability of the 5-5' and 8-5'-*SR/RS*
180 dimers.

181

182 2.2.2 *Cross-coupled diferuloylputrescine and coniferyl alcohol*

183 The radical coupling reactions of diferuloylputrescine and coniferyl alcohol are as shown in
184 Figure 4. The most exergonic of these involve C-O bonds formed through the β' -O-4 and 8-O-4'
185 linkages. Intermediate are the 8-5' and β' -5 linkages that entail bonding between an sp^3 carbon
186 and an aromatic carbon. The least exergonic of the cross-coupling reactions is through the 5-5'
187 position, in which both carbons are aromatic. In addition to differences in connectivity, the more
188 exergonic of these retain more aromatic character, resulting in increased stability. In cases for
189 which chiral centers are generated there are small differences ($0.6 \text{ kcal mol}^{-1}$, or less) with
190 stereochemistry.

191
192 The trend of energetics for the rearomatization reactions, as seen before, is the reverse of that for
193 the radical coupling, with the 5-5' product the most exergonic. Intermediate are the 8-5' and β' -5
194 products in which a new ether bond is formed along with ring closure. The least exergonic are
195 the acyclic β' -O-4 and 8-O-4' products. Among the 8-5' and β' -5 dimers, which contain
196 phenylcoumaran rings, the low-energy stereoisomers correspond to the *trans* configuration that,
197 as previously noted, is typical in the lignin polymer as well as in analogous neolignans.

198
199 The optimized geometries for the cross-coupled dimers are shown in Figure 5. Due to the smaller
200 size of coniferyl alcohol, these are less folded than the homo-coupled diferuloylputrescine
201 dimers, but there are several instances in which aromatic ring stacking can be observed. Perhaps
202 the most prominent of these occur in the *RR/SS* stereoisomer of the 8-5' dimer. The A-C rings are
203 in a parallel displaced arrangement with a plane angle of 9.76° , but the separation at 4.86 \AA is
204 greater than seen in the benzene dimer (Sinnokrot and Sherrill, 2004). The 5-5' dimer also
205 exhibits a parallel displaced conformation, with rings A and C forming a plane angle of 9.53° at

206 a separation of 3.50 Å. Although somewhat organized, the 8-5' *RS/SR* stereoisomer, β'-O-4
207 *RR/SS* stereoisomer, and β'-5 *RS/SR* have larger plane angles of 10.23, 15.89 and 10.35°,
208 respectively. The *RS/SR* stereoisomer of the β'-O-4 dimer exhibits a T-conformation between the
209 A and B rings, with a plane angle of 88.36° and inter-ring distance of 4.84 Å, which are
210 consistent with the benzene dimer (Sinnokrot and Sherrill, 2004). The 8-O-4' and β'-5 *RR/SS*
211 dimers are irregular. The parallel conformation of the 8-5' *RR/SS* and T-conformation of the β'-
212 O-4 *RS/SR* no doubt contributes to the relative stability over their stereoisomers.

213

214 **2.3 Energies of hydrogen abstraction and bond dissociation**

215 The energies of hydrogen abstraction and bond cleavage for the homo-coupled dimers of
216 diferuloylputrescine are shown in Figure 6. The energy of dehydrogenation ranges from 73.9-
217 79.5 kcal mol⁻¹, among which the 8-5' dimers are somewhat more endergonic, averaging 78.2
218 kcal mol⁻¹ as opposed to 76.3 kcal mol⁻¹ for the 8-O-4' and 5-5' dimers. The bond dissociation
219 energies are much more variable, ranging from 47.1-144.1 kcal mol⁻¹. The lowest of these is the
220 triplet formed by cleavage of the 7-O-4' ether bond, whereas the highest, as might be predicted,
221 is the 5-5' biphenyl bond. Intermediate is the cleavage of the 8-O-4' bond forming two doublets,
222 but at higher energy (79.0 kcal mol⁻¹) due to the sp² carbon atom at position C-8.

223

224 The hydrogen abstraction and bond cleavage reactions for the cross-coupled dimers of
225 diferuloylputrescine and coniferyl alcohol are shown in Figure 7. The hydrogen abstraction
226 energies range from 73.4-80.0 kcal mol⁻¹, among which 5-5' dimers have the lowest average
227 values and the β'-O-4 dimers the highest. The analogous 8-5' and β'-5 cross-coupled dimers are
228 quite similar to each other. The energies of the hydrogen abstraction reactions from the cross-

229 coupled dimers are somewhat lower than both the corresponding homo-coupled dimers in the
230 current work, the cross-coupled dimers of piceatannol and coniferyl alcohol, and the coniferyl
231 alcohol dimer (Elder et al., 2019). The ring-opening reactions of the 8-5' and β '-5 cross-coupled
232 dimers differ with stereochemistry, but do not differ markedly from the 8-5' homo-coupled
233 dimer. Among the bond cleavage reactions generating two doublets, the highest value is, as
234 before, associated with the 5-5' dimer, but is much lower than the corresponding reaction of the
235 homo-coupled dimer. Similarly, the energy of reaction for the cleavage of the 8-O-4' cross-
236 coupled dimer of diferuloylputrescine and coniferyl alcohol at 70.2 kcal mol⁻¹ is substantially
237 lower than that of the homo-coupled dimer (79.0 kcal mol⁻¹).

238

239 **2.4 Discussion**

240 Comparing the corresponding radical coupling and rearomatization reactions between homo-
241 coupled and cross-coupled dimers of diferuloylputrescine and coniferyl alcohol, the energetics
242 are generally similar. Among the quinone methide formation reactions, the homo-coupled 8-5'
243 products are more exergonic, with larger differences between the stereoisomers. The 8-O-4'
244 reaction energies are quite similar, whereas the 5-5' di-cyclohexadienone are somewhat mixed,
245 with the homo-coupling resulting in larger differences with stereochemistry. Rearomatization of
246 the homo-coupled 8-5' dimers is less exergonic, with differences between the stereoisomers. The
247 rearomatization reaction of the 8-O-4' homo-coupled dimer is less exergonic, whereas the 5-5' is
248 somewhat more exergonic.

249

250 In comparison to similar reactions with other non-conventional lignin monomers (Elder et al.,
251 2019), the quinone methides formed by 8-O-4' homo-coupling of two piceatannol units and β -O-

252 4' cross-coupling of piceatannol with coniferyl alcohol have reaction energies of -24.7 and -24.5
253 kcal mol^{-1} , respectively, such that the latter reaction of diferuloylputrescine and coniferyl alcohol
254 is somewhat more exergonic. In work on hydroxystilbene glucosides (Elder et al., 2021), 8-O-4'
255 coupling of two hydroxystilbene glucosides was considerably less exergonic ranging from -18.4
256 to $-20.5 \text{ kcal mol}^{-1}$. The energies of reaction of hydroxystilbene glucosides cross-coupled with
257 coniferyl alcohol are consistent with the current work, whereas the rearomatization energies are
258 somewhat more exergonic. Rearomatization energies of other combinations are more exergonic
259 than those in which diferuloylputrescine is the lignin monomer, but the former can result in the
260 formation of six-membered ring benzodioxanes rather than the acyclic 8-O-4' and β' -O-4
261 linkages in the current work.

262
263 The energies of reaction for quinone methide formation through the 8-5'/5'- β linkage among the
264 hydroxystilbene glucosides vary from -14.6 to $-26.7 \text{ kcal mol}^{-1}$, such that those involving
265 diferuloylputrescine are intermediate. Rearomatization energies are similar in the -30 to -40
266 kcal mol^{-1} range.

267
268 As mentioned in the Results section, the *cis* configuration of the phenylcoumaran ring resulting
269 from 8-5' homo-coupling of diferuloylputrescine is found to be the more stable stereoisomer. In
270 contrast, for the 8-5' and β -5' cross-coupled dimers the *trans* stereoisomer is more stable.
271 Experimental results, however, have routinely found that phenylcoumaran rings in lignin are in
272 the *trans* configuration (Li et al., 1997; Ralph et al., 2009).

273

274 Although it might be fortuitous if the calculated results were in agreement with experiment, it
275 must be borne in mind that the formation of dimers is a multi-step process involving radical
276 formation, coupling, and rearomatization. Based on a review of quinone methides in
277 lignification, there are still questions about which of these is the rate-determining step and if
278 dimer formation is under thermodynamic or kinetic control (Ralph et al. 2009). Furthermore, the
279 preponderance of *trans* stereochemistry in lignin notwithstanding, direct evidence for the
280 configuration of dimers involving diferuloylputrescine is not available. If for the sake of
281 argument, however, it is assumed that the rearomatization is the rate-determining step, results for
282 which the *cis* configuration is more stable would provide circumstantial evidence for kinetic
283 control.

284

285 With respect to interunit linkages, previous experimental work on the cross-coupling of coniferyl
286 alcohol with ethyl ferulate (Zhang et al., 2009) has reported on the occurrence of β -O-4', β -5' and
287 8-5' combinations, but 8-O-4' and 5-5' were not detected. For the sake of completeness, the
288 current work includes the latter documenting their thermodynamic feasibility to show that they
289 could occur with coniferyl alcohol-diferuloylputrescine cross-couples while awaiting
290 experimental results.

291

292 The energies of reactions that have been reported throughout the current paper have exclusively
293 involved neutral products and reactants. Furthermore, all results are from gas-phase calculations.
294 The latter is justified by the former as the energetics of neutral species are less sensitive to
295 solvation than for ionic reactions. That notwithstanding, it is acknowledged that solvation could
296 have an effect on conformation and, in turn, the energetics. It was found, however, that with

297 solvation the diferuloylputrescine monomer and its radical retained the folded and highly parallel
298 conformation observed in the gas phase. Optimally, any differences between computational and
299 experimental results, such as seen in the configuration of 8-5' homo-coupled
300 diferuloylputrescine, could be obviated by the use of even higher-level calculations with
301 solvation. Computational studies, such as the current one, are always a compromise between the
302 ideal calculations and the practical issues of computer time and memory requirements, especially
303 for structures of the size examined in this work. It is anticipated that as technology and
304 computational methods advance such work can be revisited and the results reassessed, ideally
305 with additional experimental data.

306

307 **3. Conclusions**

308 As discussed in the Introduction, additional evidence of cross-coupling, and the nature thereof,
309 between diferuloylputrescine and lignin awaits further experimental confirmation. This
310 notwithstanding, the current work demonstrates the thermodynamic feasibility of such reactions,
311 finding values for radical coupling and rearomatization that are similar to those found for other
312 non-conventional lignin monomers and the canonical monolignols. Furthermore, the energies of
313 the dehydrogenation reactions, essential for incorporation into the lignin polymer are generally
314 consistent with previously reported values for both monolignols and alternative lignin
315 monomers. These results show that there is no thermodynamic impediment to the formation of
316 bonds between diferuloylputrescine and monolignols and that, once formed, such coupling
317 products could feasibly undergo the subsequent dehydrogenation step needed for true
318 polymerization. With respect to conformation, particularly for the highly folded
319 diferuloylputrescine, it must be borne in mind that the current calculations have been carried out

320 on isolated molecules in which pi-stacking and other non-bonded interactions may be dominant.
321 It is acknowledged that within the complex cell wall environment, interactions could occur with
322 other, particularly aromatic, moieties potentially altering the conformation. At the present time,
323 however, information describing the composition and orientation of the constituents of the cell
324 wall at the atomistic level is not available. Future advances in detailed cell wall structure are
325 anticipated that will allow for such interactions to be taken into account in ongoing
326 computational efforts.

327

328 **4. Experimental**

329 The reactions of diferuloylputrescine examined in the current study are as shown in Figures 3
330 and 4. The initial step (Figure 1) is concerned with the oxidation of diferuloylputrescine, whereas
331 quinone methide formation through radical coupling and rearomatization of the homo-coupled
332 and diferuloylputrescine cross-coupled with coniferyl alcohol dimers are shown in Figures 3 and
333 4, respectively. As enantiomers have identical physical properties, other than the rotation of
334 plane polarized light, calculations were performed on one set of enantiomers, in structures with
335 chiral carbons.

336

337 Due to the number of rotatable bonds, these structures can exhibit considerable flexibility, such
338 that a conformational search is essential for identifying stable conformations. This was
339 accomplished using a 5000-step Monte Carlo search and optimization with the Merck force field
340 (MMFF) after which conformations within 50 kJ mol⁻¹ of the minimum were optimized with the
341 PM6 semi-empirical method as implemented in Spartan'18 (Spartan'18, 2018). The 20 low-
342 energy conformations were further refined using the M06-2X density functional method with the

343 6-31+G(d) basis set and the GD3 empirical dispersion correction. The lowest energy
344 conformation from this step was finally optimized with M06-2X/6-311++G(d,p), the GD3
345 empirical dispersion and a frequency calculation at 298.15 K to verify the identification of a
346 local minimum and for thermal corrections to the electronic energy. The density functional
347 theory calculations were all performed with Gaussian 16 (Frisch et al., 2019), using default
348 optimization criteria and the ultrafine integration grid. The values reported throughout are Gibbs
349 free energy at 289.15 K. For the coupling reactions shown in Figures 3 and 4, the radical
350 reactants were modeled as neutral doublets and all other closed-shell products as neutral singlets.
351 The optimized geometries of the dimers were used as the starting structures for the
352 dehydrogenation reactions and bond dissociation energy calculations. Appropriate hydrogens and
353 bonds were removed followed by geometry optimization of the open-shell products, such that the
354 nearest local minimum is identified. For ring-opening reactions the interatomic distance was
355 started at 2.5 Å to prevent reformation of the salient bond. The dehydrogenation products and
356 ring opened products, shown in Figures 6 and 7, were modeled as neutral doublets and neutral
357 triplets, respectively. Solvation effects of water on the geometry of diferuloylputrescine were
358 evaluated at the M062X/6-311++G(d,p) level of theory using the SMD method.

359 **Acknowledgments:**

360 This work used the Extreme Science and Engineering Discovery Environment (XSEDE), which
361 is supported by National Science Foundation grant number ACI-1548562. Specifically, it used
362 the Bridges system at the Pittsburgh Supercomputing Center (PSC), Comet at the San Diego
363 Supercomputer Center and Stampede2 at the Texas Advanced Computing Center (TACC), both
364 via MCB-090159. This work was also made possible in part by a grant of high performance
365 computing resources and technical support from the Alabama Supercomputer Authority. JR and

366 HK were funded by the DOE Great Lakes Bioenergy Research Center (DOE Office of Science
367 BER DE-SC0018409). JRe and JcDR were funded by the Spanish Projects PID2020-118968RB-
368 I00 and AGL2017-83036-R (financed by Agencia Estatal de Investigación, AEI and
369 Fondo Europeo de Desarrollo Regional, FEDER), and by the Junta de Andalucía (project P20-
370 00017). This research was supported in part by the U.S. Department of Agriculture, U.S. Forest
371 Service.

372

373

374 **Supporting Information:**

375 Cartesian coordinates for low energy conformation of all compounds, optimized using M06-
376 2X/6-311++G(d,p)

377

378 **Declaration of Interest:** The authors declare that they have no conflicts of interest.

379

380

381 **References**

382

383 Bauer, J.L., Harbaum-Piayda, B., Schwarz, K., 2012. Phenolic compounds from hydrolyzed and
384 extracted fiber-rich by-products. *LWT - Food Sci. Technol.* 47, 246–254.

385 <https://doi.org/10.1016/j.lwt.2012.01.012>

386 Bauer, J.L., Harbaum-Piayda, B., Stöckmann, H., Schwarz, K., 2013. Antioxidant activities of
387 corn fiber and wheat bran and derived extracts. *LWT - Food Sci. Technol.* 50, 132–138.

388 <https://doi.org/10.1016/j.lwt.2012.06.012>

389 Berstis, L., Elder, T., Crowley, M., Beckham, G.T., 2016. Radical nature of C-lignin. *ACS*
390 *Sustain. Chem. Eng.* 4, 5327–5335. <https://doi.org/10.1021/acssuschemeng.6b00520>

391 Berstis, L., Elder, T., Dixon, R., Crowley, M., Beckham, G., 2020. Coupling of Flavonoid
392 Initiation Sites with Monolignols Studied by Density Functional Theory. *ACS Sustain.*

393 *Chem. Eng.* 9, 1518–1528. <https://doi.org/10.1021/acssuschemeng.0c04240>

394 Chen, F., Tobimatsu, Y., Havkin-Frenkel, D., Dixon, R.A., Ralph, J., 2012. A polymer of caffeyl
395 alcohol in plant seeds. *Proc. Natl. Acad. Sci. U. S. A.* 109, 1772–1777.

396 <https://doi.org/10.1073/pnas.1120992109>

397 del Río, J.C., Marques, G., Rencoret, J., Martínez, Á.T., Gutiérrez, A., 2007. Occurrence of
398 naturally acetylated lignin units. *J. Agric. Food Chem.* 55, 5461–5468.
399 <https://doi.org/10.1021/jf0705264>

400 del Río, J.C., Rencoret, J., Gutierrez, A., Elder, T., Kim, H., Ralph, J., 2020. Lignin monomers
401 from beyond the canonical monolignol biosynthetic pathway – Another brick in the wall.
402 *ACS Sustain. Chem. Eng.* 8, 4997–5012. <https://doi.org/10.1021/acssuschemeng.0c01109>

403 del Río, J.C., Rencoret, J., Gutiérrez, A., Kim, H., Ralph, J., 2018. Structural characterization of
404 lignin from maize (*Zea mays* L.) fibers: Evidence for diferuloylputrescine incorporated into
405 the lignin polymer in maize kernels. *J. Agric. Food Chem.* 66, 4402–4413.
406 <https://doi.org/10.1021/acs.jafc.8b00880>

407 del Río, J.C., Rencoret, J., Gutiérrez, A., Kim, H., Ralph, J., 2017. Hydroxystilbenes Are
408 Monomers in Palm Fruit Endocarp Lignins. *Plant Physiol.* 174, 2072–2082.
409 <https://doi.org/10.1104/pp.17.00362>

410 del Río, J.C., Rencoret, J., Gutiérrez, A., Lan, W., Kim, H., Ralph, J., 2021. Lignin monomers
411 derived from the flavonoid and hydroxystilbene biosynthetic pathways, in: Reed, J.D., de
412 Freitas, V.A.P., Quideau, S. (Eds.), *Recent Advances in Polyphenol Research, Volume 7*,
413 Wiley Online Books. John Wiley & Sons Ltd, pp. 177–206.
414 <https://doi.org/https://doi.org/10.1002/9781119545958.ch7>

415 del Río, J.C., Rencoret, J., Marques, G., Gutiérrez, A., Ibarra, D., Santos, J.I., Jiménez-Barbero,
416 J., Zhang, L., Martínez, Á.T., 2008. Highly acylated (acetylated and/or *p*-coumaroylated)
417 native lignins from diverse herbaceous plants. *J. Agric. Food Chem.* 56, 9525–9534.
418 <https://doi.org/10.1021/jf800806h>

419 del Río, J.C., Rencoret, J., Prinsen, P., Martínez, A.T., Ralph, J., Gutiérrez, A., Martínez, Á.T.,
420 Ralph, J., Gutiérrez, A., 2012. Structural characterization of wheat straw lignin as revealed
421 by analytical pyrolysis, 2D-NMR, and reductive cleavage methods. *J. Agric. Food Chem.*
422 60, 5922–5935. <https://doi.org/10.1021/jf301002n>

423 Elder, T., Berstis, L., Beckham, G.T., Crowley, M.F., 2016. Coupling and reactions of 5-
424 hydroxyconiferyl alcohol in lignin formation. *J. Agric. Food Chem.* 64, 4742–4750.
425 <https://doi.org/10.1021/acs.jafc.6b02234>

426 Elder, T., Carlos del Río, J., Ralph, J., Rencoret, J., Kim, H., Beckham, G.T., 2019. Radical
427 coupling reactions of piceatannol and monolignols: A density functional theory study.
428 *Phytochemistry* 164, 12–23. <https://doi.org/10.1016/j.phytochem.2019.04.003>

429 Elder, T., del Río, J.C., Ralph, J., Rencoret, J., Kim, H., Beckham, G.T., Crowley, M.F., 2020.
430 Coupling and reactions of lignols and new lignin monomers: A density functional theory
431 study. *ACS Sustain. Chem. Eng.* 8, 11033–11045.
432 <https://doi.org/10.1021/acssuschemeng.0c02880>

433 Elder, T., Rencoret, J., del Río, J.C., Kim, H., Ralph, J., 2021. Radical coupling reactions of
434 hydroxystilbene glucosides and coniferyl alcohol: A density functional theory study. *Front.*
435 *Plant Sci.* 12, 1–13. <https://doi.org/10.3389/fpls.2021.642848>

436 Frisch, M.J., Trucks, G.W., Schlegel, H.B., Scuseria, G.E., Robb, M. a., Cheeseman, J.R.,
437 Scalmani, G., Barone, V., Petersson, G. a., Nakatsuji, H., Li, X., Caricato, M., Marenich, a.
438 V., Bloino, J., Janesko, B.G., Gomperts, R., Mennucci, B., Hratchian, H.P., Ortiz, J. V.,
439 Izmaylov, a. F., Sonnenberg, J.L., Williams, Ding, F., Lipparini, F., Egidi, F., Goings, J.,
440 Peng, B., Petrone, A., Henderson, T., Ranasinghe, D., Zakrzewski, V.G., Gao, J., Rega, N.,
441 Zheng, G., Liang, W., Hada, M., Ehara, M., Toyota, K., Fukuda, R., Hasegawa, J., Ishida,
442 M., Nakajima, T., Honda, Y., Kitao, O., Nakai, H., Vreven, T., Throssell, K., Montgomery

443 Jr., J. a., Peralta, J.E., Ogliaro, F., Bearpark, M.J., Heyd, J.J., Brothers, E.N., Kudin, K.N.,
444 Staroverov, V.N., Keith, T. a., Kobayashi, R., Normand, J., Raghavachari, K., Rendell, a.
445 P., Burant, J.C., Iyengar, S.S., Tomasi, J., Cossi, M., Millam, J.M., Klene, M., Adamo, C.,
446 Cammi, R., Ochterski, J.W., Martin, R.L., Morokuma, K., Farkas, O., Foresman, J.B., Fox,
447 D.J., 2019. Gaussian 16, Revision C.01, Gaussian, Inc., Wallingford CT, 2019.

448 Karlen, S.D., Smith, R.A., Kim, H., Padmakshan, D., Bartuce, A., Mobley, J.K., Free, H.C.A.,
449 Smith, B.G., Harris, P.J., Ralph, J., 2017. Highly decorated lignins in leaf tissues of the
450 canary island date palm *Phoenix canariensis*. *Plant Physiol.* 175, 1058–1067.
451 <https://doi.org/10.1104/pp.17.01172>

452 Karlen, S.D., Zhang, C., Peck, M.L., Smith, R.A., Padmakshan, D., Helmich, K.E., Free, H.C.A.,
453 Lee, S., Smith, B.G., Lu, F., Sedbrook, J.C., Sibout, R., Grabber, J.H., Runge, T.M.,
454 Mysore, K.S., Harris, P.J., Bartley, L.E., Ralph, J., 2016. Monolignol ferulate conjugates are
455 naturally incorporated into plant lignins. *Sci. Adv.* 2.
456 <https://doi.org/10.1126/sciadv.1600393>

457 Kim, E.O., Min, K.J., Kwon, T.K., Um, B.H., Moreau, R.A., Choi, S.W., 2012. Anti-
458 inflammatory activity of hydroxycinnamic acid derivatives isolated from corn bran in
459 lipopolysaccharide-stimulated Raw 264.7 macrophages. *Food Chem. Toxicol.* 50, 1309–
460 1316. <https://doi.org/10.1016/j.fct.2012.02.011>

461 Kim, H., Li, Q., Karlen, S.D., Smith, R.A., Shi, R., Liu, J., Yang, C., Tunlaya-Anukit, S., Wang,
462 J.P., Chang, H.-M.M., Sederoff, R.R., Ralph, J., Chiang, V.L., 2020. Monolignol benzoates
463 incorporate into the lignin of transgenic *Populus trichocarpa* depleted in C3H and C4H.
464 *ACS Sustain. Chem. Eng.* 8, 3644–3654. <https://doi.org/10.1021/acssuschemeng.9b06389>

465 Kim, M.J., Kim, S.M., Im, K.R., Yoon, K.S., 2010. Effect of hydroxycinnamic acid derivatives
466 from corn bran on melanogenic protein expression. *J. Appl. Biol. Chem.* 53, 422–426.
467 <https://doi.org/10.3839/jksabc.2010.065>

468 Kim, S., Chmely, S.C., Nimlos, M.R., Bomble, Y.J., Foust, T.D., Paton, R.S., Beckham, G.T.,
469 2011. Computational study of bond dissociation enthalpies for a large range of native and
470 modified Lignins. *J. Phys. Chem. Lett.* 2, 2846–2852. <https://doi.org/10.1021/jz201182w>

471 Kudanga, T., Nugroho Prasetyo, E., Sipilä, J., Eberl, A., Nyanhongo, G.S., Guebitz, G.M., 2009.
472 Coupling of aromatic amines onto syringylglycerol β -guaiacyl ether using *Bacillus SF* spore
473 laccase: A model for functionalization of lignin-based materials. *J. Mol. Catal. B Enzym.*
474 61, 143–149. <https://doi.org/10.1016/j.molcatb.2009.06.003>

475 Lan, W., Lu, F., Regner, M., Zhu, Y., Rencoret, J., Ralph, S.A., Zakai, U.I., Morreel, K.,
476 Boerjan, W., Ralph, J., 2015. Tricin, a flavonoid monomer in monocot lignification. *Plant*
477 *Physiol.* 167, 1284–1295. <https://doi.org/10.1104/pp.114.253757>

478 Lan, W., Morreel, K., Lu, F., Rencoret, J., del Río, J.C., Voorend, W., Vermerris, W., Boerjan,
479 W.A., Ralph, J., 2016a. Maize Tricin-Oligolignol Metabolites and their Implications for
480 Monocot Lignification. *Plant Physiol.* 171, pp.02012.2016.
481 <https://doi.org/10.1104/pp.16.02012>

482 Lan, W., Rencoret, J., Lu, F., Karlen, S.D., Smith, B.G., Harris, P.J., del Río, J.C., Ralph, J.,
483 2016b. Tricin-lignins: occurrence and quantitation of tricin in relation to phylogeny. *Plant J.*
484 88, 1046–1057. <https://doi.org/10.1111/tpj.13315>

485 Li, S., Ilieski, T., Lundquist, K., Wallis, A.F.A., 1997. Reassignment of relative stereochemistry
486 at C-7 and C-8 in arylcoumaran neolignans. *Phytochemistry* 46, 929–934.
487 [https://doi.org/10.1016/S0031-9422\(97\)00360-9](https://doi.org/10.1016/S0031-9422(97)00360-9)

488 Lu, F., Karlen, S.D., Regner, M., Kim, H., Ralph, S.A., Sun, R.C., Kuroda, K. ichi, Augustin,

489 M.A., Mawson, R., Sabarez, H., Singh, T., Jimenez-Monteon, G., Zakaria, S., Hill, S.,
490 Harris, P.J., Boerjan, W., Wilkerson, C.G., Mansfield, S.D., Ralph, J., 2015. Naturally *p*-
491 hydroxybenzoylated lignins in palms. *Bioenergy Res.* 8, 934–952.
492 <https://doi.org/10.1007/s12155-015-9583-4>

493 Mahmoud, A.B., Danton, O., Kaiser, M., Han, S., Moreno, A., Abd Algaffar, S., Khalid, S., Oh,
494 W.K., Hamburger, M., Mäser, P., 2020. Lignans, amides, and saponins from *Haplophyllum*
495 *tuberculatum* and Their Antiprotozoal Activity. *Molecules* 25, 2825.
496 <https://doi.org/10.3390/molecules25122825>

497 Mellon, J.E., Moreau, R.A., 2004. Inhibition of aflatoxin biosynthesis in *Aspergillus flavus* by
498 diferuloylputrescine and *p*-coumaroylferuloylputrescine. *J. Agric. Food Chem.* 52, 6660–
499 6663. <https://doi.org/10.1021/jf040226b>

500 Moreau, R.A., Hicks, K.B., 2005. The composition of corn oil obtained by the alcohol extraction
501 of ground corn. *JAOCs, J. Am. Oil Chem. Soc.* 82, 809–815.
502 <https://doi.org/10.1007/s11746-005-1148-4>

503 Moreau, R.A., Nuñez, A., Singh, V., 2001. Diferuloylputrescine and *p*-coumaroyl-
504 feruloylputrescine, abundant polyamine conjugates in lipid extracts of maize kernels. *Lipids*
505 36, 839–844. <https://doi.org/10.1007/s11745-001-0793-6>

506 Negrel, J., Pollet, B., Lapiere, C., 1996. Ether-linked ferulic acid amides in natural and wound
507 periderms of potato tuber. *Phytochemistry* 43, 1195–1199. [https://doi.org/10.1016/S0031-9422\(96\)00500-6](https://doi.org/10.1016/S0031-9422(96)00500-6)

509 Niwa, T., Doi, U., Osawa, T., 2003. Inhibitory activity of corn-derived bisamide compounds
510 against α -glucosidase. *J. Agric. Food Chem.* 51, 90–94. <https://doi.org/10.1021/jf020758x>

511 Ralph, J., Hatfield, R.D., Piquemal, J., Yahiaoui, N., Pean, M., Lapiere, C., Boudet, A.M., 1998.
512 NMR characterization of altered lignins extracted from tobacco plants down-regulated for
513 lignification enzymes cinnamyl-alcohol dehydrogenase and cinnamoyl-CoA reductase.
514 *Proc. Natl. Acad. Sci. U. S. A.* 95, 12803–12808. <https://doi.org/10.1073/pnas.95.22.12803>

515 Ralph, J., Kim, H., Lu, F., Smith, R.A., Karlen, S.D., Nuoendagula, Eugene, A., Liu, S., Sener,
516 C., Ando, D., Chen, M., Li, Y., Landucci, L.L., Ralph, S.A., Timokhin, V.I., Rencoret, J.,
517 del Río, J.C., 2021. Lignins and lignification: New developments and emerging concepts,
518 in: Quideau, S. (Ed.), *Recent Advances in Polyphenol Research, Volume 8*. John Wiley &
519 Sons Ltd, in press.

520 Ralph, J., Lapiere, C., Boerjan, W., 2019. Lignin structure and its engineering. *Curr. Opin.*
521 *Biotechnol.* 56, 240–249. <https://doi.org/10.1016/j.copbio.2019.02.019>

522 Ralph, J., Lapiere, C., Lu, F., Marita, J.M., Pilate, G., Van Doorselaere, J., Boerjan, W.,
523 Jouanin, L., 2001. NMR evidence for benzodioxane structures resulting from incorporation
524 of 5-hydroxyconiferyl alcohol into lignins of O-methyltransferase-deficient poplars. *J.*
525 *Agric. Food Chem.* 49, 86–91. <https://doi.org/10.1021/jf001042+>

526 Ralph, J., MacKay, J.J., Hatfield, R.D., O'Malley, D.M., Whetten, R.W., Sederoff, R.R., 1997.
527 Abnormal lignin in a loblolly pine mutant. *Science (80-)*. 277, 235–239.
528 <https://doi.org/10.1126/science.277.5323.235>

529 Ralph, J., Schatz, P.F., Lu, F., Kim, H., Akiyama, T., Nelsen, S.F., 2009. Quinone Methides in
530 Lignification. *Quinone Methides* 385–420. <https://doi.org/10.1002/9780470452882.ch12>

531 Rencoret, J., Kim, H., Evaristo, A.B., Gutiérrez, A., Ralph, J., del Río, J.C., 2018. Variability in
532 lignin composition and structure in cell walls of different parts of macaúba (*Acrocomia*
533 *aculeata*) palm fruit. *J. Agric. Food Chem.* 66, 138–153.
534 <https://doi.org/10.1021/acs.jafc.7b04638>

535 Rencoret, J., Neiva, D., Marques, G., Gutiérrez, A., Kim, H., Gominho, J., Pereira, H., Ralph, J.,
536 Del Río, J.C., 2019. Hydroxystilbene glucosides are incorporated into Norway spruce bark
537 lignin. *Plant Physiol.* 180, 1310–1321. <https://doi.org/10.1104/pp.19.00344>
538 Sangha, A.K., Davison, B.H., Standaert, R.F., Davis, M.F., Smith, J.C., Parks, J.M., 2014.
539 Chemical factors that control lignin polymerization. *J. Phys. Chem. B* 118, 164–170.
540 <https://doi.org/10.1021/jp411998t>
541 Sangha, A.K., Parks, J.M., Standaert, R.F., Ziebell, A., Davis, M., Smith, J.C., 2012. Radical
542 coupling reactions in lignin synthesis: A density functional theory study. *J. Phys. Chem. B*
543 116, 4760–4768. <https://doi.org/10.1021/jp2122449>
544 Sinnokrot, M.O., Sherrill, C.D., 2004. Highly accurate coupled cluster potential energy curves
545 for the benzene dimer: Sandwich, T-shaped, and parallel-displaced configurations. *J. Phys.*
546 *Chem. A* 108, 10200–10207. <https://doi.org/10.1021/jp0469517>
547 Spartan'18, 2018. Spartan'18 Wavefunction, Inc. Irvine, CA.
548 Vanholme, R., De Meester, B., Ralph, J., Boerjan, W., 2019. Lignin biosynthesis and its
549 integration into metabolism. *Curr. Opin. Biotechnol.* 56, 230–239.
550 <https://doi.org/10.1016/j.copbio.2019.02.018>
551 Yoshimura, M., Ochi, K., Sekiya, H., Tamai, E., Maki, J., Tada, A., Sugimoto, N., Akiyama, H.,
552 Amakura, Y., 2017. Identification of characteristic phenolic constituents in mousouchiku
553 extract used as food additives. *Chem. Pharm. Bull.* 65, 878–882.
554 <https://doi.org/10.1248/cpb.c17-00401>
555 Zhang, A., Lu, F., Sun, R., Ralph, J., 2009. Ferulate-coniferyl alcohol cross-coupled products
556 formed by radical coupling reactions. *Planta* 229, 1099–1108.
557 <https://doi.org/10.1007/s00425-009-0894-6>
558 Zhao, Y., Truhlar, D.G., 2008. The M06 suite of density functionals for main group
559 thermochemistry, thermochemical kinetics, noncovalent interactions, excited states, and
560 transition elements: Two new functionals and systematic testing of four M06-class
561 functionals and 12 other function. *Theor. Chem. Acc.* 120, 215–241.
562 <https://doi.org/10.1007/s00214-007-0310-x>
563
564
565

566 **Figure captions**

567

568 Figure 1. Diferuloylputrescine and resonance structures from dehydrogenation.

569

570 Figure 2. Optimized geometries for diferuloylputrescine, the diferuloylputrescine radical (with
571 spin densities) and homo-coupled diferuloylputrescine dimers.

572

573 Figure 3. Gibbs free energies of reaction for radical coupling to form quinone methides and
574 rearomatization for homo-coupled diferuloylputrescine dimers.

575

576 Figure 4. Gibbs free energies of reaction for radical coupling to form quinone methides and
577 rearomatization for cross-coupled diferuloylputrescine-coniferyl alcohol dimers.

578

579 Figure 5. Optimized geometries for cross-coupled diferuloylputrescine-coniferyl alcohol dimers.

580

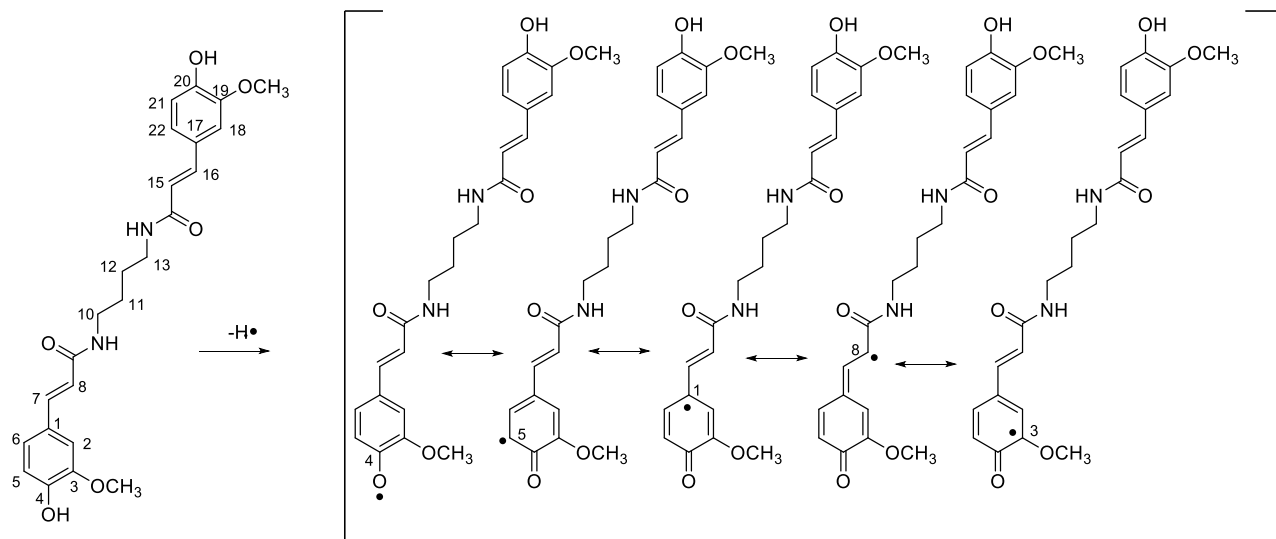
581 Figure 6. Gibbs free energy of reaction for dehydrogenation and bond dissociation of homo-
582 coupled diferuloylputrescine dimers.

583

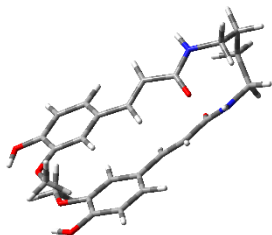
584 Figure 7. Gibbs free energy of reaction for dehydrogenation and bond dissociation of cross-
585 coupled diferuloylputrescine-coniferyl alcohol dimers.

586

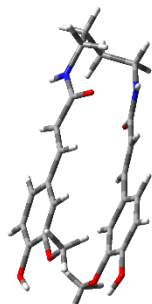
587
588
589



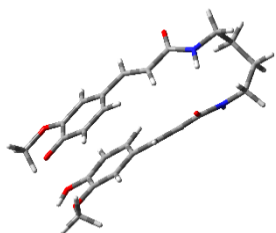
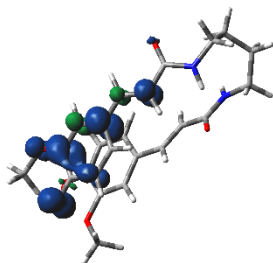
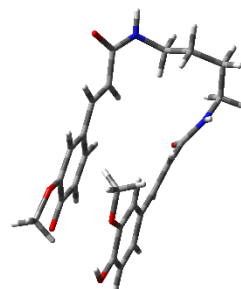
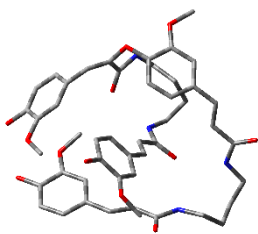
590
591
592
593



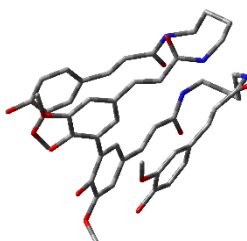
diferuloylputrescine



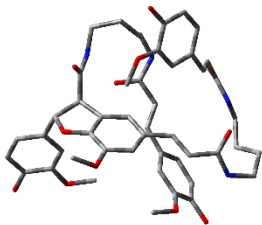
diferuloylputrescine solvated

diferuloylputrescine
radicaldiferuloylputrescine
radical spin densitydiferuloylputrescine
radical solvated

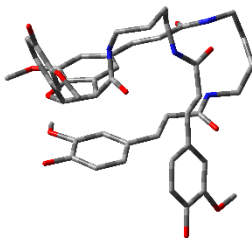
8-O-4'



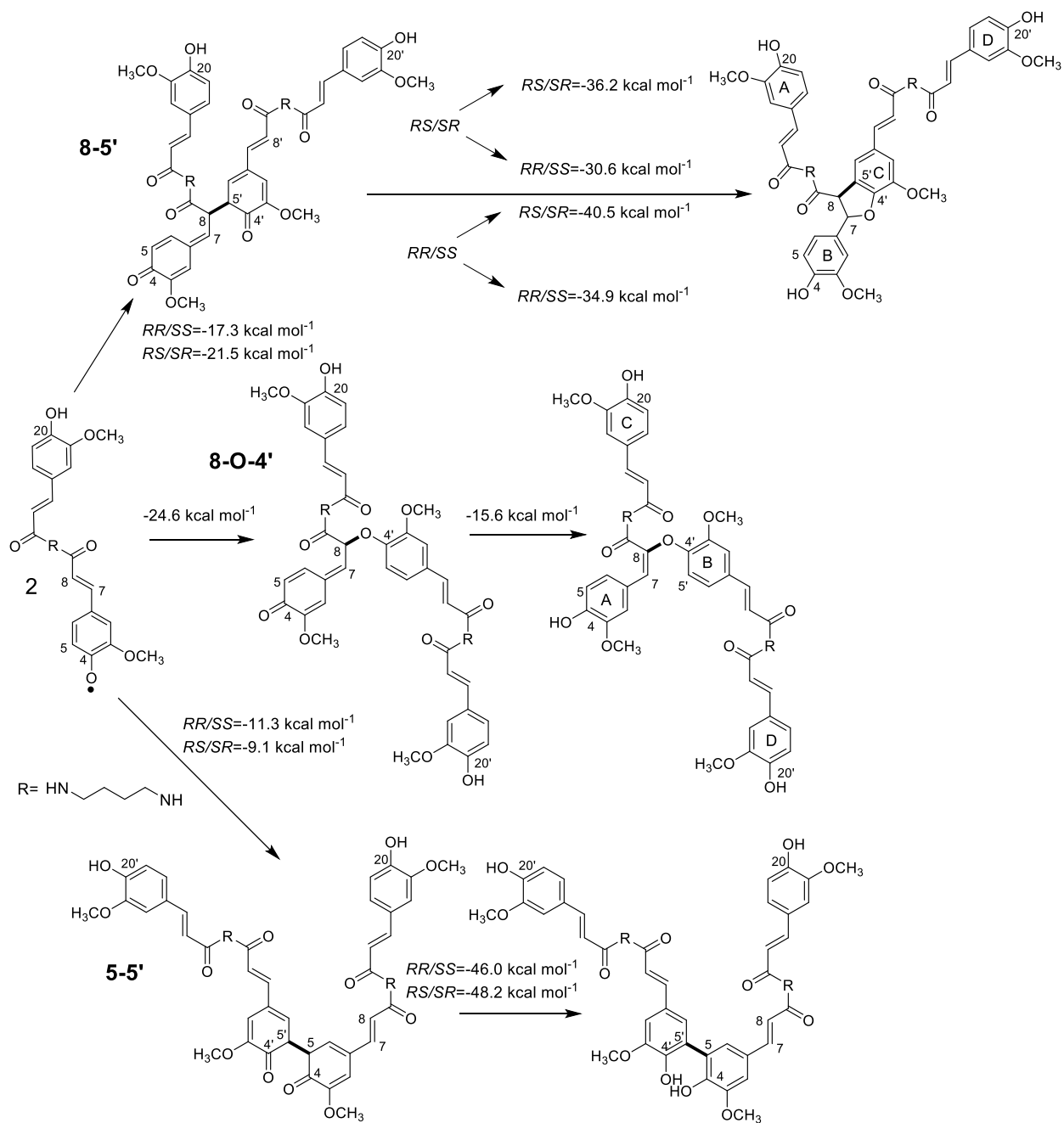
5-5'



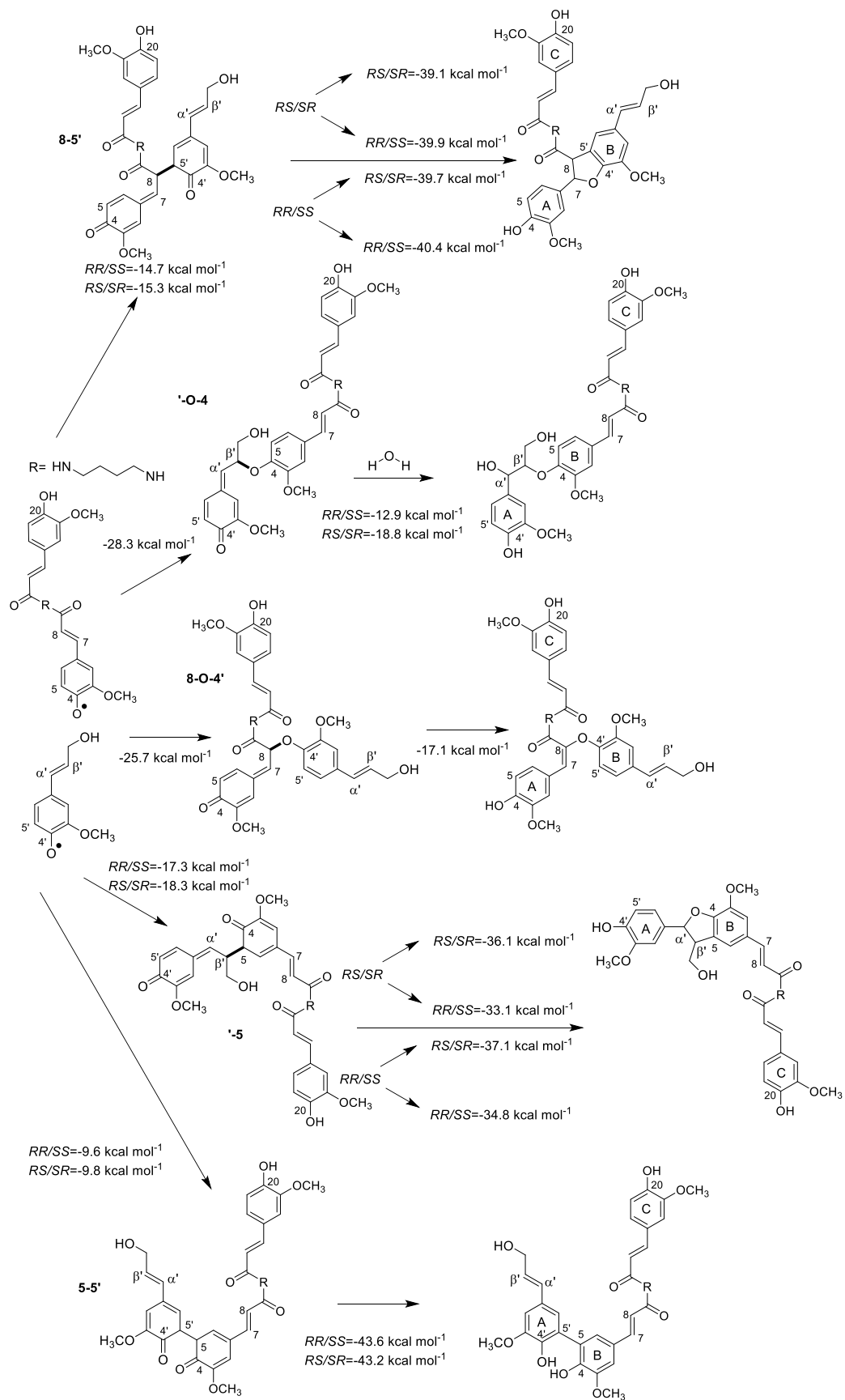
8-5' (SS/RR)

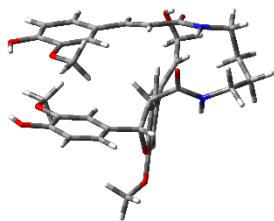
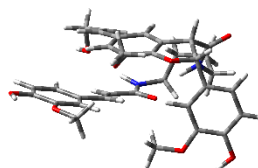
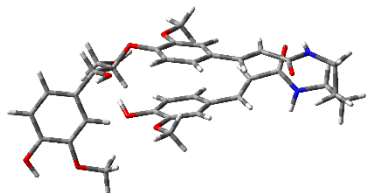
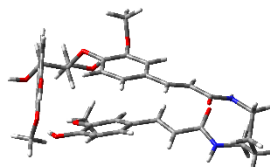
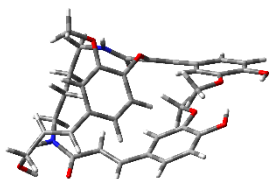


8-5' (RS/SR)

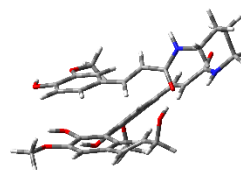


598
599
600
601
602
603

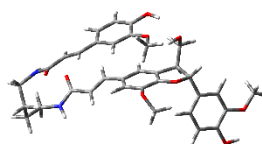


8-5' (*SS/RR*)8-5' (*RS/SR*) β' -O-4 (*SS/RR*) β' -O-4 (*RS/SR*)

8-O-4'



5-5'

 β' -5 (*SS/RR*) β' -5 (*RS/SR*)

